Published in final edited form as:
Nat Catal. 2018 March 8; 1(3): 208–213. doi:10.1038/s41929-018-0037-1.

Redox tuning the Weakley-type polyoxometalate archetype for the oxygen evolution reaction

Mercè Martin-Sabi[#1], **Joaquín Soriano-López**[#2], **Ross S. Winter**[1], **Jia-Jia Chen**[1], **Laia Vilà-Nadal**[1], **De-Liang Long**[1], **José Ramón Galán-Mascarós**[2,3,*], and **Leroy Cronin**[1,*]

[1]WestCHEM, School of Chemistry, University of Glasgow, Glasgow, UK

[2]Institut Català d'Investigació Química (ICIQ), Tarragona, Spain

[3]ICREA, Barcelona, Spain

[#] These authors contributed equally to this work.

Abstract

Water oxidation is a key reaction for the conversion of solar energy into chemical fuels, but effective water-oxidation catalysts are often based on rare and costly precious metals such as Pt, Ir or Ru. Developing strategies based on earth-abundant metals is important to explore critical aspects of this reaction, and to see whether different and more efficient applications are possible for energy systems. Herein, we present an approach to tuning a redox-active electrocatalyst based on the doping of molybdenum into the tungsten framework of $[Co_4(H_2O)_2(PW_9O_{34})_2]^{10-}$, known as the Weakley sandwich. The Mo-doped framework was confirmed by X-ray crystallography, electrospray ionization mass spectrometry and inductively coupled plasma optical emission spectrometry studies. The doping of molybdenum into the robust Weakley sandwich framework leads to the oxidation of water at a low onset potential, and with no catalyst degradation, whereby the overpotential of the oxygen evolution reaction is lowered by 188 mV compared with the pure tungsten framework.

Natural photosynthesis is able to store solar energy in a chemical fuel by powering the oxidation of water to form NADPH, the reduced form of nicotinamide adenine dinucleotide phosphate, and O_2 (ref. 1). However, energy conversion schemes based on sunlight really use water splitting into both H_2 and O_2, an uphill energy transformation involving multielectron transfer events2,3,4,5. Given the abundance of water, hydrogen production6 using electrolysis should be cheap as many effective hydrogen evolution catalysts have been reported7. However, hydrogen production is not straightforward as it is coupled with the slower water-oxidation process3. Hence, the energetic cost of obtaining oxygen via water oxidation is the rate-limiting step for obtaining hydrogen (see equation (1), E^0 is the standard electrode potential)3. Therefore, the development of water-oxidation catalysts

[*] jrgalan@iciq.es; Lee.Cronin@glasgow.ac.uk.

Data availability

The datasets generated during and analysed during the current study are available from the corresponding author on reasonable request. Crystallographic data (excluding structure factors) have been deposited with the Cambridge Crystallographic Data Centre (CCDC 1563819–1563824) and may be obtained free of charge via www.ccdc.cam.ac.uk/data_request/cif. Full synthetic, analytical, crystallographic and topological analyses are given in the Supplementary Information.

Europe PMC Funders Author Manuscripts

(WOCs) beyond examples that use precious metals, for example, IrO_2, is a critical step to produce hydrogen cheaply and at scale8. An ideal WOC must be fast, capable of water oxidation at a potential minimally above the thermodynamic value, and display oxidative, hydrolytic and thermal stability.

$$2H_2O(l) \rightarrow 2H_2(g) + O_2(g) E^0 = 1.23V \quad (1)$$

Given this challenge, much effort has been put into the synthesis of earth-abundant-based WOCs, mostly based on stable bulk metal oxides1and molecular species9,10,11,12,13,14,15. As first-row transition metals are abundant, less toxic and able to catalyse several reactions16, they can yield inexpensive WOC catalysts that operate under homogeneous conditions9,11,12,13,17, based, for instance, on cobalt oxides13 and iron9,17. Cobalt-containing WOCs are formed under oxidizing conditions from aqueous $Co_{(II)}$ salts, and operate at moderate potentials and are oxidatively stable1. The stability of polyoxometalates (POMs) against oxidation makes them excellent candidates to develop artificial photosystems that can operate over long periods of time. However, there are few examples of POMs based on first-row transition metals capable of performing effectively as WOCs18,19. Perhaps one of the most remarkable examples is the cobalt-containing POM framework $[Co_4(H_2O)_2(PW_9O_{34})_2]^{10-}$ recently reported by Hill et al.20,21, which is the well-known stable Weakley-sandwich archetype22 (Fig. 1). In fact, the Co-POM WOCs are fast and efficient, but POMs form complex mixtures and mechanistic investigations so far have only been able to explore the nature of the catalyst under different conditions, for example, heterogeneous or homogeneous, varying pH and inclusion of electroactive additives19. Tungsten-based POMs are stable and have expanded the library of WOCs19,22,23,24,25,26, although many of them still contain precious metals such as the ruthenium substituted $\{Ru_4Si_2W_{20}\}$ POM by Bonchio et al.27,28. The lifetime and catalytic activity of $\{Ru_4Si_2W_{20}\}$ opened a new paradigm in WOCs. In this context, our hypothesis was to implement the Weakley sandwich as a catalyst archetype that could be doped with different metals to tune its redox properties and improve its catalytic activity and stability. In fact, multimetallic catalysis has already been used to improve the homogeneous catalytic oligomerization of ethylene, and to lower the effective voltages needed to drive oxygen evolution reactions29. Crucially, we deployed the doped material as a heterogeneous electrocatalyst and analysed the parent $\{Co_4W_{18}\}$ under identical conditions for a direct comparison of properties.

Herein we show that it is possible to dope molybdenum into the $[Co_4(H_2O)_2(PW_9O_{34})_2]^{10-}$ = $\{Co_4W_{18}\}$ structure22 synthesizing a mixed Mo and W $\{Co_4Mo_xW_y\}$ Weakley sandwich, a well known, easy to synthesize POM cluster that is a known WOC. Using this approach, we were able to tune the amount of Mo doped into the structure, gain positional control and lower the overpotential for water oxidation by 188 mV, achieving 517 mV versus 705 mV for the undoped parent $\{Co_4W_{18}\}$ compound. WOCs often decompose to other active materials under moderate applied potentials, challenging the nature of the genuine catalytic species30. This problem is often overcome by immobilizing the molecular WOCs on electrode surfaces31,32,33,34. The structurally robust WOC $\{Co_4Mo_xW_y\}$ shows a

high degree of oxidative stability and is able to be anchored to the electrode. Our system has fully succeeded in combining the high efficiency and tunability of a molecular catalyst with the durability and stability of a bulk material in a heterogeneous electrocatalyst for water oxidation. In this study, we have shown that a mixture of Mo/W shows a high activity towards water oxidation with an stability comparable to cutting-edge bulk metal oxide catalysts. Structural mapping shows the preferential distribution of doped molybdenum near the catalytic active site adjacent to the terminal water ligands at the end of the $\{Co_4\}$ core, and electrospray ionization mass spectrometry (ESI-MS) analysis confirms that the compounds are mixtures of differently substituted $\{Mo_xW_y\}$ species. This results show how solid solutions of redox-active metals can be used to tailor the catalytic properties of well-known cluster-catalyst archetypes.

Results

Synthesis of the Mo-doped Weakley sandwich $\{Co_4Mo_xW_y\}$

The synthesis of the tungsten and cobalt-containing Weakley sandwich-type POM is a straightforward, one-pot reaction, giving yields over 35%. The procedure involves heating CO^{2+}, phosphate and tungstate salts in a 2:1:9 ratio in water at reflux22. The strategy was to dope the synthesis of the traditional $\{Co_4W_{18}\}$ with different amounts of molybdenum. The following percentages of molybdenum in the reaction were tested: 10, 20, 30, 40, 50, 60, 70, 80, 90 and 100. The synthetic procedure consisted of mixing the molybdate and tungstate salts in the presence of a phosphate salt, then lowering the pH to 6.5 by addition of acetic acid. This solution was added to a cobalt solution and the resulting mixture was refluxed for 2 h. After that, potassium acetate was added to promote crystallization and the resulting brown liquor was left to crystallize. All the reactions yielded two types of crystals after one day except for the three highest molybdenum percentages, which only formed precipitate on ongoing evaporation. However, only reactions using three molybdenum percentages were reliably reproducible in a good yield, those being 40% (compound **1**), 50% (compound **2**) and 60% (compound **3**). The two types of crystals were big dark brown block crystals (‘type A’ compounds **1a**–**3a**) and small golden rectangles (‘type B’ compounds **1b**–**3b**).

Electrochemistry of the Mo-doped Weakley sandwich {Co4Mo x W y}

Cation exchange from the Na/K^+ salts into Cs^+ was performed to yield water insoluble compounds **1a[Cs]**, **1b[Cs]**, **2a[Cs]**, **2b[Cs]**, **3a[Cs]** and **3b[Cs]** for heterogeneous catalysis studies to be conducted. These were also analysed by inductively coupled plasma optical emission spectrometry (ICP-OES), which showed that the Mo:W ratio was maintained relative to the Na/K^+ salts. Electrochemical experiments were performed to determine the effect of the molybdenum substitution into the cluster and assess the water-oxidation properties of the compounds (**1a[Cs]**–**3a[Cs]** and **1b[Cs]**–**3b[Cs]**). Nafion–carbon black inks of the compounds were prepared and deposited onto the surface of a glassy carbon electrode to conduct the electrochemical measurements. Linear sweep voltammetry was performed on these salts (pH 7 in 50 mM KPi buffer, 0.8–1.4 V versus Ag/AgCl) to determine whether there was an electrochemical difference between them. As can be seen in Fig. 2a,b the onset potential for water oxidation decreases as the proportion of molybdenum

increases in the cluster, with **3a[Cs]** and **3b[Cs]** being the best catalysts for each type of cluster (see Tafel plots, Fig. 3a,b).

To explore the differences in the catalytic activity of compounds **1a[Cs]**, **1b[Cs]**, **2a[Cs]**, **2b[Cs]**, **3a[Cs]** and **3b[Cs]** using modified electrodes (using Nafion binder and carbon black), rotating linear sweep voltammetry experiments were conducted to determine the differences in the onset potentials among compounds **1a[Cs]**, **1b[Cs]**, **2a[Cs]**, **2b[Cs]**, **3a[Cs]** and **3b[Cs]**. The caesium salt of the all-tungsten material ({$Co_4(PW_9)2$}) was also tested as a control experiment (see Fig. 2). At a current density of 1 mA cm^{-2} the potential for the water splitting of **3b**[**Cs**] is reduced by 188 mV compared with the pure tungsten Weakley. Type A materials (Fig. 2a,c) show that **3a[Cs]** has the lowest onset potential, followed by **2a[Cs]** (these two range between 1.30 and 1.35 V). They are followed by **1a[Cs]**, which has an onset potential of ~1.35 V. These values are much lower compared with the all-tungsten analogue, which has an onset potential higher than 1.40 V. Type B materials (Fig. 2b,d) also follow the same tendency, with **3b[Cs]** the material showing the lowest onset potential, followed by **2b[Cs]** and **1b[Cs]** (the three compounds show an onset potential between 1.30 and 1.35 V).

There are remarkable current density differences between type A and type B compounds at a given potential. At 1.6 V, **1a[Cs]** shows a current density slightly higher than 2.5 mA cm^{-2}, and **1b[Cs]** displays a current density of almost 4.0 mA cm^{-2}. At 1.5 V, **2a[Cs]** has a current density of almost 2.5 mA cm^{-2} and **2b[Cs]** has one of that is slightly higher than 3.0 mA cm^{-2}. Finally, at 1.4 V, **3a[Cs]** shows a current density value slightly higher than 1.5 mA cm^{-2} and **3b[Cs]** has a current density of almost 3.5 mA cm^{-2}. Meaning that in general, type B compounds are faster than type A compounds in catalysing the water-oxidation reaction. This observation is in agreement with the experimental data; the Tafel data show that type B materials have faster kinetics than type A materials. As compounds **3a[Cs]** and **3b[Cs]** showed the best performances as catalysts for the water-oxidation reaction, deeper electrochemical analysis was performed on these two materials.

Bulk electrolysis experiments using compounds **3a[Cs]** and **3b[Cs]** were performed to test their hydrolytic and oxidative stability when used as catalysts as part of Nafion inks (see Fig. 2c for **3a[Cs]** and Fig. 2d for **3b[Cs]**). Chronoamperometry was performed on compounds **3a[Cs]** and **3b[Cs]** at 1.4 V versus Ag/AgCl (1.6 V versus normal hydrogen electrode (NHE)). The experiments were conducted in 40 ml of pH 7.1 buffer, in a single cell. A steady current density of of 0.4 mA cm^{-2} was achieved after 1.5 h, kept constant for >12 h, and gas bubbles were seen to form the working electrodes during these experiments. During these experiments, the current density was constant, suggesting that both **3a[Cs]** and **3b[Cs]** remained stable. In addition, inspection of the working electrodes after the experiments revealed no change in the surface material. Also, studies with steady-state current at different potentials were done on modified glassy carbon electrodes with the inks prepared using **3a[Cs]** and **3b[Cs]**.

Multistep chronoamperometry was conducted on compounds **3a[Cs]** and **3b[Cs]** and a Tafel plot was produced for each catalyst (Fig. 3). Compound **3a[Cs]** shows a Tafel slope of 217 mV $decade^{-1}$ and an overpotential of 648 mV at 1 mA cm^{-2}. Compound **3b[Cs]** shows a

Tafel slope of 228 mV decade^{-1} and an overpotential of 620 mV at 1 mA cm^{-2}. Such high Tafel slope values have been previously reported, but they are not associated with this work, as the compounds that show these high slopes are structurally and chemically very different. All compounds show an improved water-oxidation capability relative to the all-tungsten {Co_4W_{18}} parent, demonstrating that doping molybdenum into the tungsten framework of the cluster is a good strategy for improving the catalytic activity of POM WOCs. The materials obtained from one crystal form or the other (type A versus type B) exhibit slightly different, but significant, catalytic behaviour, with compounds **1b[Cs]**, **2b[Cs]** and **3b[Cs]** showing a lower onset potential for oxygen evolution than **1a[Cs]**, **2a[Cs]** and **3a[Cs]**, respectively. The reasons for the variation are not completely understood as compounds **1a**–**3a** and **1b**–**3b** have the same ratio of Mo/W; however, there are minor cationic differences between compounds **1a**–**3a** and **1b**–**3b**, which may be the attributing factor for these electrochemical variations. A detailed mechanistic study is not the aim of the present work, but recent work on a tetracobalt-polyoxometalate catalyst suggests that active cobalt oxides {$Co^{II}_4O_4$} as WOCs undergo oxidation to Co^{III} (ref. 35). A similar study suggested that the active {$Co^{II}_4O_4$} cubane is the most efficient heterogeneous Co-oxide WOC and the Co/Ni-cubane bridges homogeneous and heterogeneous catalyst design through fine-tuned edge-site environments of the Co centres36.

The best candidates for splitting water, compounds **3a[Cs]** and **3b[Cs]**, were studied for stability and oxygen evolution performance. To further investigate the qualities of the mixture of Mo and W compounds, bulk electrolysis was conducted at 1.4 V versus Ag/AgCl for 12 h (Fig. 2c,d), showing that both compounds can give a steady current for relatively long periods of time, proving their stability and performance at pH 7. To confirm the Faradaic oxygen production during bulk electrolysis, we monitored the oxygen evolution in the gas space in analogous pH and buffered conditions. For these experiments, we used carbon paste electrodes instead (see Supplementary Information section 4)34, to achieve higher current densities and, therefore, to detect the presence of oxygen more easily. Chronopotentiometry for **3a[Cs]** and **3b[Cs]** was conducted at a constant current of 1 mA cm^{-2} (Fig. 3c,d). The oxygen evolved data are quantitative when compared with the expected amount of generated oxygen. Thus, we can rule out the participation of competitive reactions. This guarantees that the data acquired by this process are a good parameter to assess the electrocatalytic activity of these materials.

Solution stability and characterization of {$Co_4Mo_xW_y$}

The stability of compounds in solution was determined by electrospray ionization ion mobility mass spectrometry (ESI-IM-MS) on the six compounds (see Fig. 4 and Supplementary Tables 5–10). Assigning specific species to the peak envelopes proved difficult due to significant envelope overlapping. Therefore, using this particular technique allowed for the separation of species not only by the mass/charge ratio (m/z), but also by their cross-sectional area. The six compounds display similar profiles via ESI-IM-MS. At a first glance, the profiles for compounds **1a**, **2a** and **3a** appeared to be very similar. However compounds **2a** and **3a** seem to have their envelopes shifted to lower m/z values, indicating that the species present in these samples are lighter. This agrees with the fact that

compounds **2a** and **3a** have a higher percentage of the lighter element Mo. A similar trend was observed for compounds **1b**, **2b** and **3b** (see Supplementary Tables 5–10).

The signals at $m/z < 900$ correspond to fragments of the parent cluster. Above $m/z = 900$, two differently charged series can be observed. A major one at $m/z = \sim 1{,}000$ with a charge of −4 and a minor one with a centre between $m/z = 1{,}200$ and 1,300. On the plots of drift time versus m/z, it can be clearly seen that the −4 and −3 signals correspond to different species, whose spectra can be separated. The difference in the envelopes of the −4 group of envelopes suggests that there are multiple $\{Co_4Mo_xW_y\}$ species present incorporating different ratios of Mo/W, such as $\{Mo_7W_{11}\}$, $\{Mo_8W_{10}\}$ and $\{Mo_9W_9\}$ (see Supplementary Tables 5–10 for specific assignments). The −3 group of envelopes is much broader and also corresponds to the fully intact $\{Co_4M_{18}\}$ sandwich. A wider range of species can be assigned to this signal than the −4 group of envelopes. In some cases, peaks represent the mixed addenda from the $\{Co_4Mo_6W_{12}\}$ species to the $\{Co_4Mo_{18}\}$ cluster. Identification of the $\{Co_4Mo_{18}\}$ cluster is virtually unprecedented, as such a structure based on all-molybdenum lacunary fragments is exceptionally rare37.

Complementary to mass spectrometry, ICP-OES results helped to definitively assess the molybdenum content. ICP-OES was conducted on the six different samples obtained (**1a**, **1b**, **2a**, **2b**, **3a** and **3b**) to determine the proportion of molybdenum to tungsten in each material. Despite their almost identical unit-cell parameters, compounds **1**–**3** were chemically distinct, with a unique Mo:W ratio; however, between crystal types A and B, the Mo:W ratio was largely conserved. However, there was a slight variation in the countercations present. The ICP results showed that the synthetic ratio did not match the final ratio of the products. A lower amount of molybdenum compared with the synthetic ratio was found in the crystals, meaning that not all the molybdenum available is introduced into the structure. As expected, reactions with a higher percentage of molybdenum produced compounds with correspondingly higher Mo content (Table 1). Overall, the MS analysis gave a good indication that the compounds obtained are crystalline mixtures of multiple Weakley sandwich clusters of varying Mo:W ratios, and the formula obtained via ICP-OES represents the average ratio of all these different clusters.

Crystallography of the Mo-doped Weakley sandwich {Co4Mo x W y}

To fully explore the structural composition of the new compounds, single-crystal X-ray crystallography was conducted to identify the positional preferences of Mo and W atoms within the doped Weakley sandwich structure. Compounds **1a**–**3a** crystals belong to the monoclinic system ($P2_1/n$ space group) and have the following unit cell dimensions:

$a = 12.8$ Å, $b = 16.5$ Å, $c = 21.5$ Å, $\alpha = 90°$, $\beta = 104°$, $\gamma = 90°$, $V = \sim 4{,}393$ Å^3.

Compounds **1b**–**3b** belong to the triclinic system ($P\bar{1}$ space group). Compounds **1b** and **2b** have the following unit cell dimensions:

$a = 11.5$ Å, $b = 13.2$ Å, $c = 18.2$ Å, $\alpha = 70°$, $\beta = 73°$, $\gamma = 73°$, $V = \sim 2{,}230$ Å^3.

However, compound **3b** has a slight change in unit cell dimensions, which are:

a = 12.3 Å, b = 13.3 Å, c = 16.2 Å, α = 101°, β = 73°, γ = 111°, V = ~2,394 Å^3.

Single-crystal X-ray structure determination revealed that compounds have the Weakley structure with C_{2h} symmetry: four cobalt atoms sandwiched by two {PM_9} POM units form a rectangle, of which two cobalt centres are on the C_2 axis with all coordination oxo ligands from the POM units. While the other two cobalt centres each have one water ligand. Structure refinements indicated that all metal (M) sites in the {PM_9} POM units contain both tungsten and molybdenum. Having C_{2h} symmetry, the whole cluster has only five unique positions for the metal sites and (average positional preferences for either W or Mo on each unique position are summarized in Fig. 5). The two unique metal sites on the cap of the {PM_9} block show a preference for tungsten with occupancy ratios of around W:Mo = 0.8:0.2. One metal site of the belt positions—that nearest the cluster centre—also prefers tungsten with an occupancy ratio of around W:Mo = 0.63:0.35. However, the remaining two unique belt positions show a preference for molybdenum with an occupancy ratio of around W:Mo = 0.35:0.65. This is interesting as the location of the maximum enrichment of the Mo is adjacent to one of the terminal water ligands on the {Co_4} belt, as shown in Fig. 5.

Discussion

In summary, we have shown that substituting molybdenum into the known {Co_4W_{18}} Weakley sandwich structure is a successful strategy towards POM-based WOCs, and structure control on these clusters has been achieved and confirmed by ICP-OES and ESI-IM-MS. The ratio of molybdenum to tungsten observed in the final compounds is lower than the ratio used synthetically, but up to the equivalent of eight of the eighteen addenda sites can be replaced reliably with molybdenum. MS revealed that the final compounds are complex crystalline mixtures of many different Mo/W containing clusters, with evidence revealing the unexpected presence of the elusive {Co_4Mo_{18}} species. The results provide a strategy for generating molecular heterogeneous catalysts by doping known W clusters with Mo to improve their WOC properties, opening up this field to the development of POM-based WOCs using similar design principles.

Methods

Materials and chemicals

All chemicals were purchased from Sigma-Aldrich and used without further purification. $Na_{10}[Co_4(H_2O)_2(PW_9O_{34})_2]$ was synthesized according to ref. 22. Detailed description of the synthesis of compounds **1a**, **1b**, **2a**, **2b**, **3a**, **3b** can be found in the Supplementery Information, section 2.

Single crystal X-ray diffraction

Suitable single crystals were selected and mounted onto the end of a thin glass fibre using Fomblin oil. Single-crystal datasets and unit cells were collected at 150(2) K on a Bruker Apex II Quasar diffractometer equipped with a graphite monochromator (λ (MoKα) = 0.71 Å) at 150(2) K. Structure solution and refinement was carried out using SHELXS-9738and SHELXL-9739 via WinGX40. Selected details of the data collection and structural

refinement of each compound can be found in Supplementary Tables 12–17 and full details are available in the corresponding .cif files.

Electrospray ionization mass spectrometry

Measurements were performed using a Waters Synapt-G2 spectrometer. The instrument was operated in negative mode and with an electrospray source regularly calibrated using 2 μg l^{-1} NaI solution in 1:1 2-propanol/H_2O from Waters Q-ToF Qualification Standard Kit. The sample was dissolved in 1:1 mixture of high-performance liquid chromatography (HPLC) grade deionized water and HPLC grade acetonitrile and injected into the spectrometer at a flow rate of 5 μl min^{-1}. The following parameters were used for acquisition of all spectra: ESI capillary voltage, 2.9 kV; sample cone voltage, 10.0 V; extraction cone voltage, 4.0 V; source temperature, 80 °C; desolvation temperature, 180 °C; cone gas (N_2) flow, 15 l h^{-1}; desolvation gas (N_2) flow, 750 l h^{-1}; source gas flow, 0.0 ml min^{-1}; trap gas flow, 2.0 ml min^{-1}; helium cell gas flow, 180 ml min^{-1}; ion-mobility spectrometry–mass spectrometry (IMS-MS) gas flow, 90.0 ml min^{-1}; IMS-MS DC entrance, 25.0; helium cell DC, 35.0; helium exit, −5.0; IMS bias, 3.0; IMS-MS DC exit, 0.0; IMS-MS wave velocity, 1,087 m s^{-1}; IMS-MS wave height, 23.7 V. Data were acquired using MassLynx v4.1 and initially processed using Waters DriftScope v2.2 software. IM-MS spectra are displayed with a linear intensity scale using the colour-coding shown in the accompanying key (Fig. 4); no filtering is applied to limit signals or remove noise. Data analysis was performed on the Waters Driftscope v2.2 software.

Inductively coupled plasma optical emission spectroscopy

The sodium and potassium compounds were dissolved in HPLC grade water without digestion. The compounds containing caesium were digested in 3 ml hydrogen peroxide and then dissolved in HPLC grade water. The instrument used was an Agilent 5100.

Electrochemistry

Measurements were made on a single-channel Bio Logic SP150 potentiostat.

Oxygen evolution

Oxygen evolution was detected with an Ocean Optics NeoFOX oxygen-sensing system equipped with a FOXY probe inserted into the gas space of the reactor, close to the anode.

Supplementary Material

Refer to Web version on PubMed Central for supplementary material.

Acknowledgements

We acknowledge J. Mathieson and D. Castro-Spencer for their kind help and support in acquiring the ESI-IM-MS data. We thank L. MacDonald for offering supportive discussion on the electrochemistry. We also thank J. M. Poblet and J. Carbò for helpful discussion on the POM design, characterization and electrocatalysis. We gratefully acknowledge financial support from the Engineering and Physical Sciences Research Council (grant nos EP/H024107/1, EP/J015156/1, EP/K021966/1, EP/L015668/1, EP/L023652/1), the European Research Council (project 670467 SMART-POM) and the University of Glasgow. This work was partially funded by the Spanish Ministerio de Economia y Competitividad (MINECO) through projects CTQ2015-71287-R and the Severo Ochoa Excellence Accreditation 2014-2018 SEV-2013-0319; the Generalitat de Catalunya (2014-SGR-797) and the

Europe PMC Funders Author Manuscripts

Centres de Recera de Catalunya Programme/Generalitat de Catalunya. We also thank Chemistry and Molecular Sciences and Technologies European Cooperation in Science & Technology Action CM1203.

References

1. Kanan MW, Nocera DG. In situ formation of an oxygen-evolving catalyst in neutral water containing phosphate and Co2+ Science. 2008; 231:1072–1075.
2. Young KJ, et al. Light-driven water oxidation for solar fuels. Coord Chem Rev. 2012; 256:2503–2520. [PubMed: 25364029]
3. Meyer TJ. Catalysis: the art of splitting water. Nature. 2008; 451:778–779. [PubMed: 18273008]
4. Eisenberg R, Gray HB. Preface on making oxygen. Inorg Chem. 2008; 47:1697–1699. [PubMed: 18330963]
5. Mazloomi K, Gomes C. Hydrogen as an energy carrier: prospects and challenges. Renew Sustain Energy Rev. 2012; 16:3024–3033.
6. Dau H, et al. Te mechanism of water oxidation: from electrolysis via homogeneous to biological catalysis. ChemCatChem. 2010; 2:724–761.
7. Zou X, Zhang Y. Noble metal-free hydrogen evolution catalysts for water splitting. Chem Soc Rev. 2015; 44:5148–5180. [PubMed: 25886650]
8. Slavcheva E, et al. Sputtered iridium oxide flms as electrocatalysts for water splitting via PEM electrolysis. Electrochim Acta. 2007; 52:3889–3894.
9. Fillol JL, et al. Efcient water oxidation catalysts based on readily available iron coordination complexes. Nat Chem. 2011; 3:807–813. [PubMed: 21941254]
10. Ruttinger W, Dismukes GC. Synthetic water-oxidation catalysts for artifcial photosynthetic water oxidation. Chem Rev. 1997; 97:1–24. [PubMed: 11848863]
11. Wasylenko DJ, Palmer RD, Berlinguette CP. Homogeneous water oxidation catalysts containing a single metal site. Chem Commun. 2013; 49:218–227.
12. Cole-Hamilton DJ. Homogeneous catalysis—new approaches to catalyst separation, recovery, and recycling. Science. 2003; 299:1702–1706. [PubMed: 12637737]
13. Evangelisti F, Güttinger R, Moré R, Luber S, Patzke GR. Closer to photosystem II: a Co4O4 cubane catalyst with fexible ligand architecture. J Am Chem Soc. 2013; 135:18734–18737. [PubMed: 24279370]
14. Brimblecombe R, Swiegers GF, Dismukes GC, Spiccia L. Sustained water oxidation photocatalysis by a bioinspired manganese cluster. Angew Chem Int Ed. 2008; 47:7335–7338.
15. Dismukes GC, et al. Development of bioinspired Mn4O4-cubane water oxidation catalysts: lessons from photosynthesis. Acc Chem Res. 2009; 42:1935–1943. [PubMed: 19908827]
16. Enthaler S, Junge K, Beller M. Sustainable metal catalysis with iron: from rust to a rising star? Angew Chem Int Ed. 2008; 47:3317–3321.
17. Ellis WC, McDaniel ND, Bernhard S, Collins TJ. Fast water oxidation using iron. J Am Chem Soc. 2010; 132:10990–10991. [PubMed: 20698652]
18. Evangelisti F, Car PE, Blacque O, Patzke GR. Photocatalytic water oxidation with cobalt-containing tungstobismutates: tuning the metal core. Catal Sci Technol. 2013; 3:3117–3129.
19. Lv H, et al. Polyoxometalate water oxidation catalysts and the production of green fuel. Chem Soc Rev. 2012; 41:7572–7589. [PubMed: 22972187]
20. Yin Q, et al. A fast soluble carbon-free molecular water oxidation catalyst based on abundant metals. Science. 2010; 328:342–345. [PubMed: 20223949]
21. Huang Z, et al. Efcient light-driven carbon-free cobalt-based molecular catalyst for water oxidation. J Am Chem Soc. 2011; 133:2068–2071. [PubMed: 21268644]
22. Weakley TJR, Evans HT, Showell JS, Tourné GF, Tourné CM. 18-Tungstotetracobalto(11)diphosphate and related anions: a novel structural class of heteropolyanions. J Chem Soc Chem Commun. 1973; 139:140.
23. Han XB, et al. Polyoxometalate-based cobalt-phosphate molecular catalysts for visible light-driven water oxidation. J Am Chem Soc. 2014; 136:5359–5366. [PubMed: 24661303]

Europe PMC Funders Author Manuscripts

24. Goberna-Ferrón S, Vigara L, Soriano-López J, Galán-Mascarós JR. Identifcation of a nonanuclear {Coii 9} polyoxometalate cluster as a homogeneous catalyst for water oxidation. Inorg Chem. 2012; 46:11707–11715.
25. Zhu G, et al. Water oxidation catalyzed by a new tetracobalt-substituted polyoxometalate complex: [{Co4(μ-OH)(H2O)3}(Si2W19O70)]11–. Dalton Trans. 2012; 41:2084–2090. [PubMed: 22186630]
26. Tanaka S, et al. Visible light-induced water oxidation catalyzed byn molybdenum-based polyoxometalates with mono- and dicobalt(iii) cores as oxygen-evolving centers. Chem Commun. 2012; 48:1653–16559.
27. Sartorel A, McDaniel ND, Bernhard S, Bonchio M. Polyoxometalate embedding of a tetraruthenium(iv)-oxo-core by template-directed metalation of [γ-SiW10O36]8–: a totally inorganic oxygen-evolving catalyst. J Am Chem Soc. 2008; 130:5006–5007. [PubMed: 18345628]
28. Sartorel A, et al. Water oxidation at tetraruthenate core stabilized by polyoxometalated ligands: experimental and computational evidence to trace the competente intermediates. J Am Chem Soc. 2009; 131:16051–16053. [PubMed: 19842627]
29. Zhang B, et al. Homogeneously dispersed multimetal oxygen-evolving catalysts. Science. 2016; 352:333–337. [PubMed: 27013427]
30. Stracke JJ, Finke RG. Electrocatalytic water oxidation beginning with the cobalt polyoxometalate [Co4(H2O)2(PW9O34)2]10–: identifcation of heterogeneous CoOx as the dominant catalyst. J Am Chem Soc. 2011; 133:14872–14875. [PubMed: 21894961]
31. Concepcion JJ, Binstead RA, Alibabaei L, Meyer TJ. Application of the rotating ring-disc-electrode technique to water oxidation by surfacebound molecular catalysts. Inorg Chem. 2013; 52:10744–10746. [PubMed: 24050703]
32. Zhong DK, Zhao SL, Polyansky DE, Fujita E. Diminished photoisomerization of active ruthenium water oxidation catalyst by anchoring to metal oxide electrodes. J Catal. 2013; 307:140–147.
33. Klepser BM, Bartlett BM. Anchoring a molecular iron catalyst to solar-responsive WO3 improves the rate and selectivity of photoelectrochemical water oxidation. J Am Chem Soc. 2014; 136:1694–1697. [PubMed: 24437445]
34. Soriano-López J, et al. Cobalt polyoxometalates as heterogeneous water oxidation catalysts. Inorg Chem. 2013; 52:4753–4755. [PubMed: 23611185]
35. Soriano-López J, et al. Tetracobalt-polyoxometalate catalysts for water oxidation: key mechanistic details. J Catal. 2017; 350:56–63.
36. Song F, et al. {Co4O4} and {CoxNi4−xO4} cubane water oxidation catalysts as surface cut-outs of cobalt oxides. J Am Chem Soc. 2017; 139:14198–14208. [PubMed: 28953394]
37. Li S, et al. Rare sandwich-type polyoxomolybdates constructed form di/ tetra-nuclear transition-metal clusters and trivacant kegging germanomolybdate fragments. Inorg Chem. 2009; 48:9819–9830. [PubMed: 19769384]
38. Sheldrick GM. A short history of SHELX. Acta Crystallogr. 2008; A64:112–122.
39. Müller P. Crystal Structure Refnement: A Crystallographer's Guide to SHELXL. Oxford Univ. Press; Oxford: 2006.
40. Farrugia LJ. WinGX and ORTEP for Windows: an update. J Appl Crystallogr. 2012; 45:849–854.

Europe PMC Funders Author Manuscripts

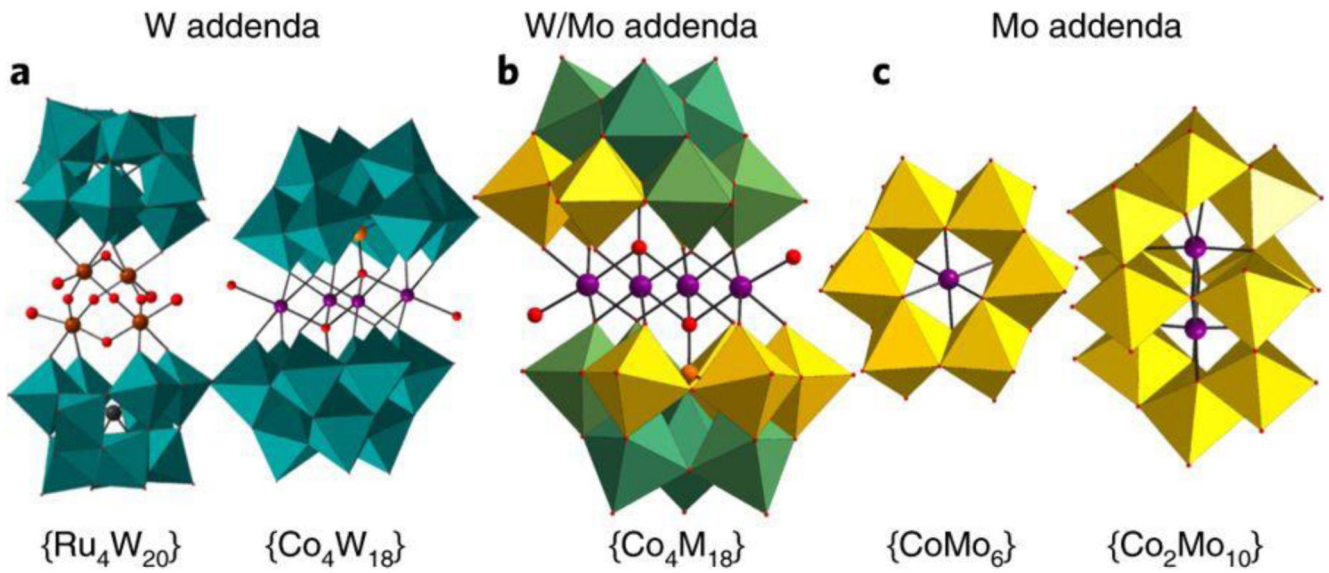

Figure 1. Polyhedral structures of earth-abundant-based WOCs.

a, Representation of two tungsten-based WOCs ({Ru_4W_{20}}27 and {Co_4W_{18}}20). **b**, Representation of the new cluster family with mixed Mo/W addenda positions. **c**, Representation of two molybdenum-based WOCs ({$CoMo_6$}26 and {Co_2Mo_{10}}26). Red spheres, oxygen; purple spheres, cobalt; brown spheres, ruthenium; orange spheres, phosphorous; grey spheres, silicon. Teal polyhedra, {WO_6} units; yellow polyhedra, {MoO_6} units; mixed teal–yellow polyhedra, {MO_6} units, where M = Mo/W.

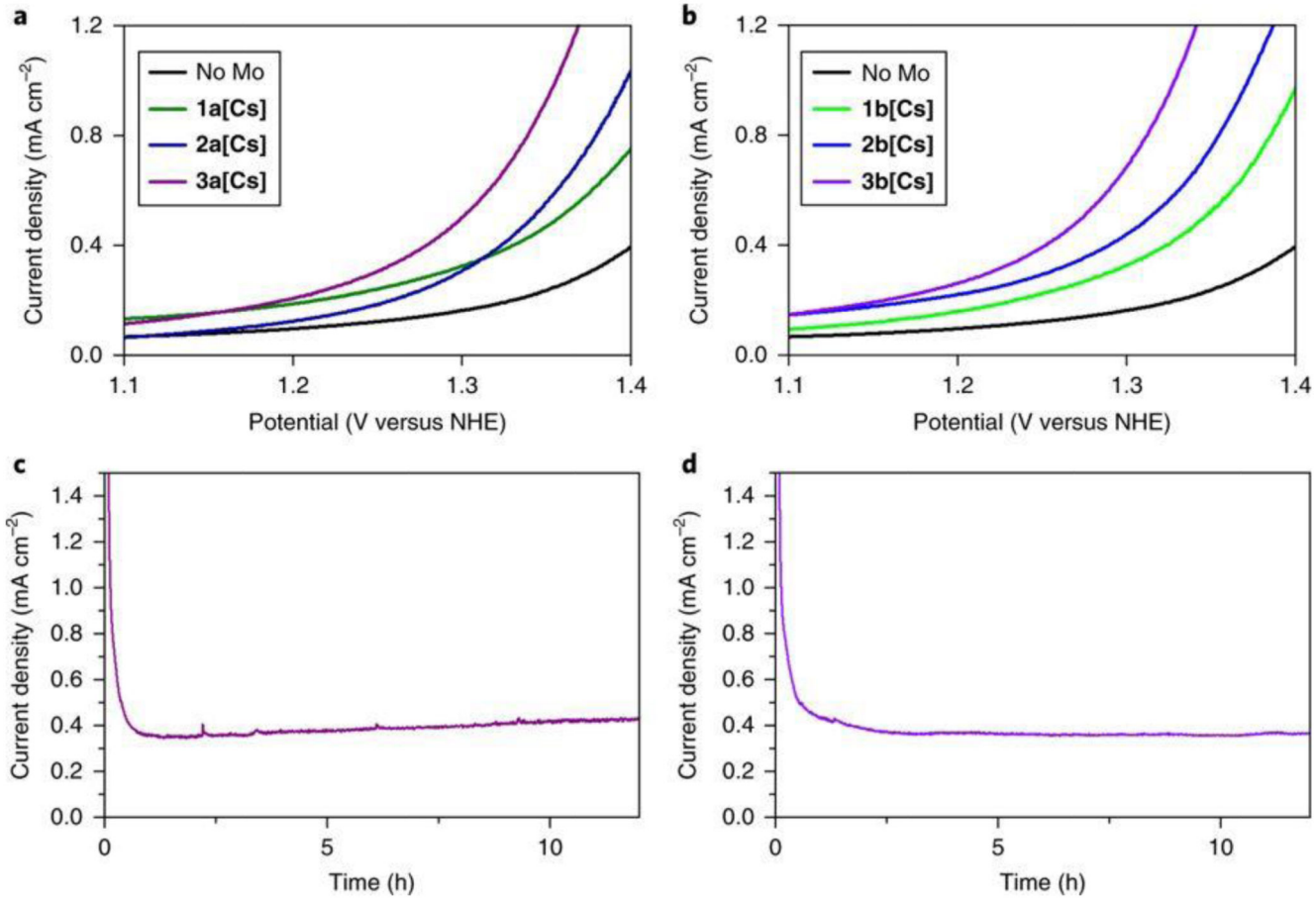

Figure 2. Electroanalytical analysis of the compounds.

a,**b**, Rotating disc electrode linear sweep voltammogram for the materials **1a[Cs]**–**3a[Cs]** and **1b[Cs]**–**3b[Cs]**, respectively. The experiment was conducted in a single cell at pH 7.1 in 50 mM KPi buffer, 1 M KNO_3. Rotating disc speed, 2,000 r.p.m. Scan rate, 2 mV s^{-1}. **c**,**d**, Bulk electrolysis of compounds **3a[Cs]** (**c**) and **3b[Cs]** (**d**) performed at pH = 7.1 in 50 mM KPi buffer, 1 M KNO_3 at 1.4 V versus Ag/AgCl.

Europe PMC Funders Author Manuscripts

Europe PMC Funders Author Manuscripts

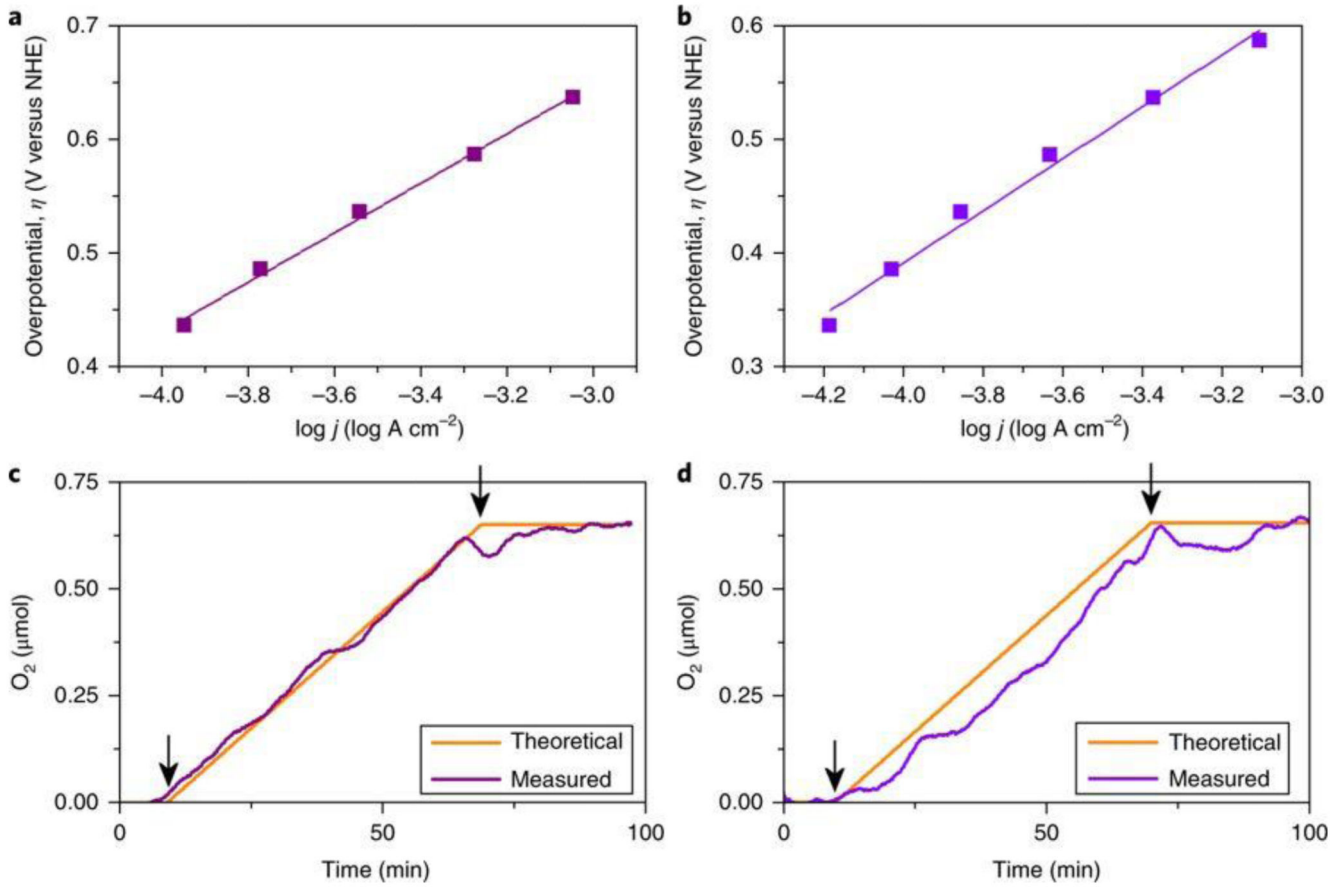

Figure 3. Electrochemical kinetics analysis of the compounds.

a,**b**, Tafel data for **3a[Cs]** (**a**) and **3b[Cs]** (**b**) extracted from doing 1 min bulk electrolysis scanning from 0.8 V to 1.4 V versus Ag/AgCl in 50 mV increments. pH 7.1, 50 mM KPi buffer, 1 M KNO_3. **c**,**d**, Oxygen evolution during bulk water electrolysis with carbon paste electrodes containing 20% weight of compounds **3a[Cs]** (**c**) and **3b[Cs]** (**d**) performed at pH 7.1 in 50 mM KPi buffer, 1 M KNO_3 at 1.4 V versus Ag/AgCl. Theoretical oxygen evolution was calculated estimating Faradaic production from current data (arrows indicate initial and final electrolysis times).

Europe PMC Funders Author Manuscripts

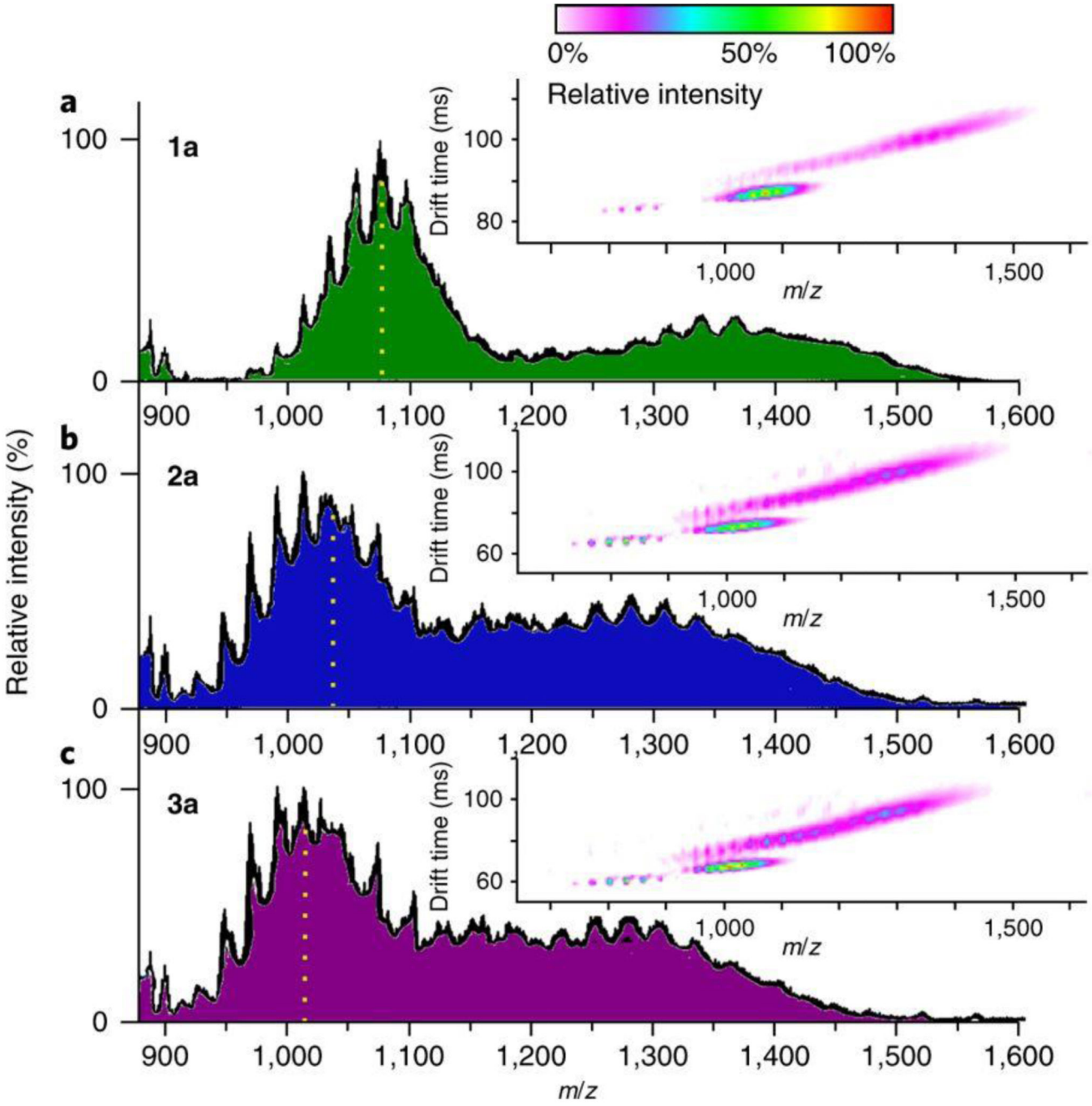

Figure 4. Mass spectrometry data showing the stability of the compounds.

a–**c**, ESI-IM-MS of compounds **1a** (**a**), **2a** (**b**) and **3a** (**c**). Left axis shows relative intensity. The insets show the drift time for the different −4 and −3 species plotted against *m/z*. The dotted vertical lines indicate the centre of the group of envelopes once separated from the –3 group of envelopes at a higher *m*/*z* value. For more information, see Supplementary Section 3.

Europe PMC Funders Author Manuscripts

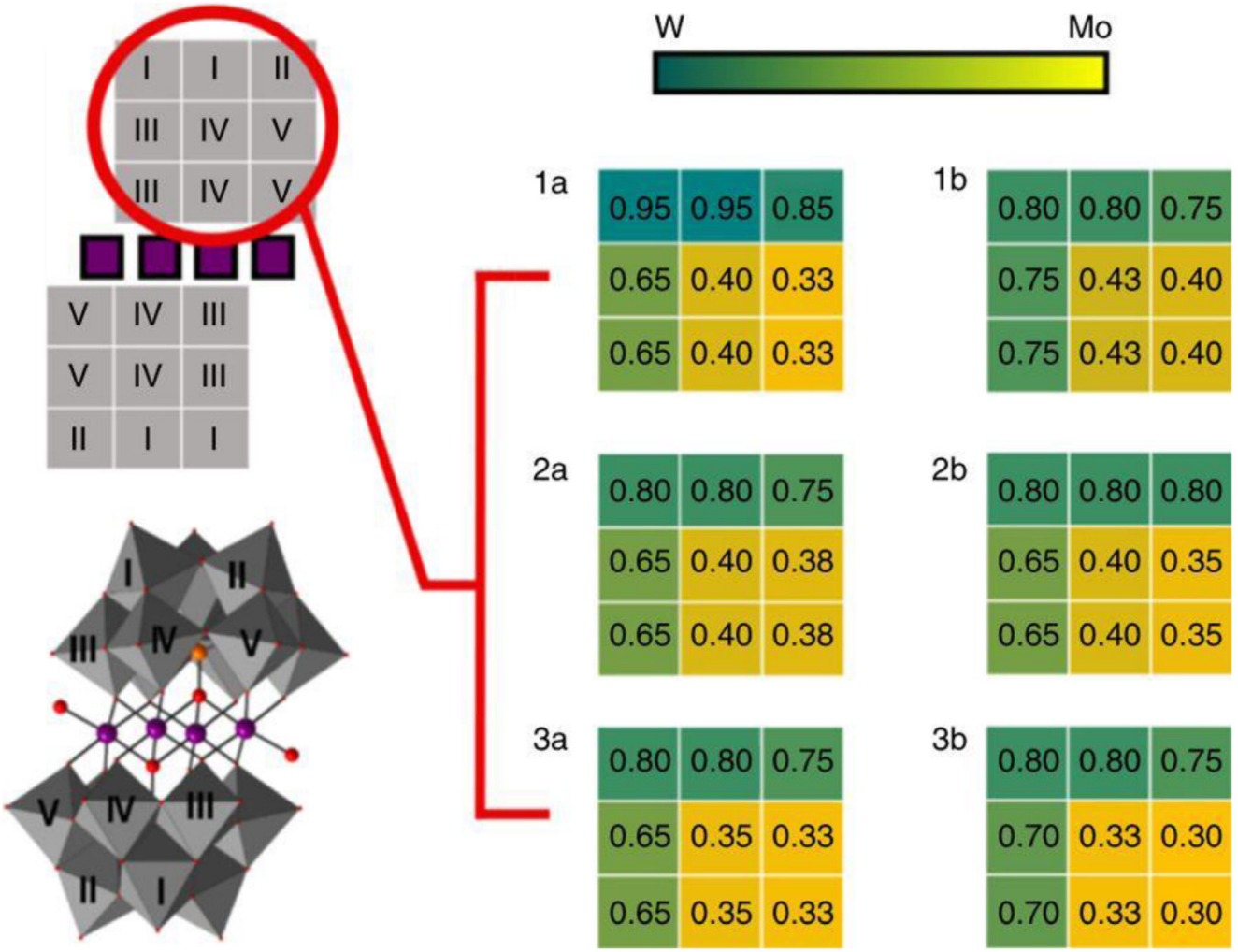

Figure 5. Crystallographic data showing site occupancy for the six compounds.

Representation of the molybdenum-doped Weakley sandwich $\{Co_4Mo_xW_y\}$ showing the crystallographically identified unique positions in both polyhedral and simple two-dimensional formats, and a heatmap representation of the tungsten occupancy across these nine, but five unique positions in one of the symmetrically linked halves of the Weakley sandwich.

Europe PMC Funders Author Manuscripts

Table 1

Comparison of the expected number of atoms of Mo:W in $\{Co_4P_2Mo_xW_yO_{68}\}$ based on the synthetic ratio used to the observed numbers found via ICP-OES

Compound (% Mo used in the synthesis)	Expected number based on synthetic ratio		Found number in formula	
	Mo	W	Mo	W
1a and **1b** (40% Mo)	7.2	10.8	7.0	11.0
2a and **2b** (50% Mo)	9.0	9.0	7.6	10.4
3a and **3b** (60% Mo)	10.8	7.2	8.0	10.0